Investigation of Networked SSHI Configurations for Plate-Based Piezoelectric Energy Harvesters

Engin Tarhan[1], Seyed Morteza Hoseyni[1], Amirreza Aghakhani[2] and Ipek Basdogan[1]

[1]Department of Mechanical Engineering, College of Engineering, Koç University, Istanbul, Turkey

[2]Institute of Biomaterials and Biomolecular Systems, University of Stuttgart, Stuttgart, Germany

Corresponding Author:

Ipek Basdogan, Department of Mechanical Engineering, College of Engineering, Koç University, 34450, Istanbul, Turkey. Email: ibasdogan@ku.edu.tr

Abstract

Piezo-patch energy harvesters attached to plate-like structures can be used to extract multimodal vibrational energy. For each piezo-patch, SSHI circuits can boost the harvested power compared to standard rectifier circuits. However, the effect of using different configurations of the SSHI network for multiple piezo-patches on plate structures has not yet been understood. This study aims to assess the performance of the networked SSHI configurations compared to networked rectifier configurations and investigate the optimum configurations for energy harvesting purposes. For this, three piezo-patches are bonded to an aluminum plate and connected to single and/or multiple circuits. The equivalent circuit model (ECM) of the electromechanical system is developed from the experimentally validated analytical model and utilized in simulation software LTspice. The performances of considered configurations are evaluated regarding peak power outputs, and the optimal load resistances are obtained. Based on the experimental findings, the best configuration is determined and verified by simulations. The results show that by using respective SSHIs, the power output can be improved by preventing charge cancellation despite the cost of increased diode loss. This study contributes to our understanding of optimal energy harvesting techniques by investigating the effectiveness of networked SSHI configurations for multiple piezo-patches on plate structures.

Keywords: Networked SSHI, Piezoelectric, Multimodal Energy Harvesting, Equivalent Circuit Model, Plate

1. Introduction

Vibration-based energy harvesting applications for the purpose of replacing conventional batteries that have certain lifetimes have received great interest over the last decade. These harvesting systems primarily aim to generate electrical power to be used in small electrical devices and components as they enable self-powered systems (Erturk and Inman, 2011). To convert this vibrational energy to electrical energy, there are several transducers that are applicable, such as electrostatic (Torres and Rincón-Mora, 2008), electromagnetic (Lee et al., 2009), piezoelectric (Erturk and Inman, 2011, Howells, 2009), magnetostrictive (Wang and Yuan, 2008, Narita and Fox, 2018) and electroactive (Graf et al., 2010). Among these, piezoelectric transduction is the most popular method of energy conversion since piezoelectric materials have large power densities, and they are easy to be manufactured and implemented at different geometries and scales (Anton and Sodano, 2007, Erturk and Inman, 2011, Li et al., 2020).

In the majority of the studies about piezoelectric energy harvesting, the piezoelectric energy harvesters are in the form of cantilevered beams because of their simple structure, with one or two layers of piezoelectric materials which are known as unimorph configuration and bimorph configuration, respectively (Erturk and Inman, 2008, Zheng et al., 2014, Elvin and Elvin, 2009a, Johnson et al., 2006, Sodano et al., 2004, Jiang et al., 2005, Friswell et al., 2012, Erturk et al., 2009, Erturk and Inman, 2009, Pradeesh et al., 2022). Although cantilever beam harvesters have been extensively investigated in the literature, they have some significant drawbacks. These drawbacks can be stated as their requirement for extra space for the fixture and the proof masses, the energy loss due to the fixture (Lee et al., 2010), and their inability to harvest the energy in a broadband form. These harvesters have to be excited at their resonance frequencies to have at least a mediocre power generation, which can also result in mechanical failures (Safaei et al., 2019).

As an alternative to beam harvesters, patch-based piezoelectric energy harvesters are more efficient and easier to implement on plate-like structures, which are widely used in many areas such as automotive, aerospace, and marine applications. These types of harvesters have larger number of vibration modes, and for that reason, energy can be harvested in a broadband frequency range. Although most studies in the literature focused on beam structures, there are several studies focusing on energy harvesting from plate-like structures. In earlier studies, researchers used a resistive load to find the AC power output (Junior et al., 2009, Aridogan et al., 2014a, Aridogan et al., 2014b, Aridogan et al., 2016). However, there are some challenges when it comes to practical purposes, like transferring the power to a storage capacitor. For practical applications, the alternating current obtained from energy harvesting should be transformed into a more stable form. For this purpose, a rectifier bridge and a smoothing capacitor can be used to transform the alternating current (AC) to a steady rectified direct current (DC). For most of these transformations, a full-wave AC-DC rectifier is used. In addition to this AC-DC transformation, it is advantageous to use a smoothing capacitor to improve the performance where the smoothing

capacitor acts as a DC-DC converter (Ottman et al., 2002). Aghakhani and Basdogan (2017) have developed an analytical model using equivalent impedance approach to predict the power output after rectification for multiple piezoelectric harvesters (MPEHs) attached on a thin plate. Although voltage regulation can be obtained by DC-DC converters, the output power is not satisfactory for some applications and could be improved further with additional circuit elements. For this purpose, Lefeuvre et al. (2005) have developed a self-adaptive circuit called synchronous electric charge extraction (SECE). Guyomar et al. (2005) proposed another technique which synchronizes the vibrations of the system and the electric charge extraction and named synchronized switch harvesting on inductor (SSHI), which increases the output power by 900% compared to standard harvesting circuit. In SSHI technique, an electrical switching device is connected to the piezoelectric elements and this device causes the system to behave in a nonlinear fashion. The working principle of the SSHI circuit is the switching device gets triggered when the mechanical displacement of the harvester reaches an extremum which leads to the quasi-instantaneous inversion of the polarity of the piezoelectric element. By the repetition of this process, the voltage is improved (Guyomar et al., 2005, Lefeuvre et al., 2004). There are numerous studies focusing on especially the circuitry of the SSHI, and these studies are summarized by Chao (2011). Recently, Hoseyni et al. (2023) developed an analytical model based on equivalent impedance approach for a piezoelectric energy harvester integrated on a thin plate with a single SSHI circuit.

In the presence of non-linear components, the electrical simulation software (e.g. LTspice) become very handy in estimating the power output of such systems. At this point, one needs another approach to model the mechanical system in such a way that the whole system can be integrated with the non-linear electrical circuit components. In this study, equivalent circuit modelling (ECM) approach is used for simulating the piezoelectric energy harvester attached on a thin-plate with AC-DC conversion via a circuit simulator software (e.g., LTspice). Related to the ECM studies in the literature, Elvin and Elvin (2009b) used Rayleigh-Ritz Method to find the equivalent circuit parameters for any number of vibration modes of a base-excited cantilever piezoelectric generator and validated their model by comparing their results with the analytical model of Erturk and Inman (2008). Elvin and Elvin (2009a) also studied a finite-element model coupled with SPICE for a conventional cantilever beam configuration with base excitation, but the data extraction and transferring the data between FEA and SPICE were difficult (Yang and Tang, 2009). Yang and Tang (2009) have also focused on cantilever piezoelectric generators and developed a more robust technique to extract the equivalent circuit parameters from a finite-element model. For plate-based applications, Bayik et al. (2016) proposed a multi-mode ECM of a piezoelectric patch attached to a thin plate and found the equivalent circuit parameters both by analytical and numerical approaches. Aghakhani and Basdogan (2017) have extended this model to MPEHs attached on a thin plate. They also integrated their ECM with a rectifier model in SPICE and validated their model both analytically and experimentally.

Although there are some studies about evaluating the performance of the SSHI circuits (Shu et al., 2009), there are limited number of studies focusing on the networked configurations of the SSHI circuits. Wu et al. (2013) have studied SSHI circuits on the improvement of vibration damping of a clamped steel plate. They have proposed two networks, which are synchronized switch damping by energy transfer (SSDT) and synchronized switch damping with diode (SSDD) and compared these networks' performances with synchronized switch damping on an inductor (SSDI) baseline. While SSDT relies on the principle of switching synchronized with the structure modal coordinates and obtaining a voltage inversion for damping, SSDD relies on the principle of orienting the energy flow by using the diode's one-way allowance of current. Both networks they proposed resulted in a better performance in terms of damping. Li et al. (2013) have studied network of the piezoelectric elements for energy harvesting purposes focusing on the first four modes. However, their study only involved numerical simulations conducted in Simulink, and the excitation was limited to pulse mode. But in pulse mode, the energy is distributed in several modes according to the structure's natural impulse response, and for different energy distributions, simply a harmonic force can be applied instead of a pulse excitation (Wu et al., 2013). In another study, Long et al. (2021) suggested that the problem related to the opposite vibration phases for the piezoelectric harvesters can be overcome by their proposed split-inductor-capacitor scheme. They carried out experiments using a full-bridge rectifier circuit, a conventional p-SSHI circuit and their newly proposed p-SSHI circuit. According to their results, they achieved a significant improvement in the power output. However, they focused mainly on the phase problem, and did not analyze the respective SSHI and rectifier circuits' performances.

The motivation of this study is to assess the performance of the networked SSHI configurations compared to networked rectifier configurations. For this research question, four different networked rectifier/SSHI configurations are presented where two of these configurations include a single rectifier/SSHI circuit, and the other two configurations include separate rectifier/SSHI circuits for each patch. The performances of the four configurations are evaluated under harmonic excitation in terms of peak power outputs both experimentally and numerically. For this purpose, the modal analysis is done using the Rayleigh-Ritz method, and the ECM approach is used to simulate the electromechanical system in SPICE software. Later, this ECM is integrated with the rectifier/SSHI circuits, and different configurations are obtained. The simulations are done for thirteen different load resistances to narrow down the load resistance steps and find the optimum load resistance for each configuration. The same configurations are developed experimentally, and the results are compared with the simulations to verify the performance trends of different networked rectifier/SSHI configurations.

2. Distributed parameter model and equivalent circuit modeling of the thin-plate with multiple piezo-patches

The model used in this study is presented in Figure 1. The plate has a length of a, a width of b and a thickness of h_p. As the thickness of the plate is too small compared to its length and width, Kirchhoff plate theory suggests that the transverse shear deformation can be neglected. All four edges of the plate are in clamped (C-C-C-C) position. A transverse point force $f(t)$ is applied at (x_0, y_0) to excite the system, where n_p is the number of piezoceramic patches. A resistive load is connected to the electrode layers of piezo-patches and denoted as R_l. The analytical model developed by Aridogan et al. (2014b) incorporates the electromechanical coupling between the patches and the thin plate.

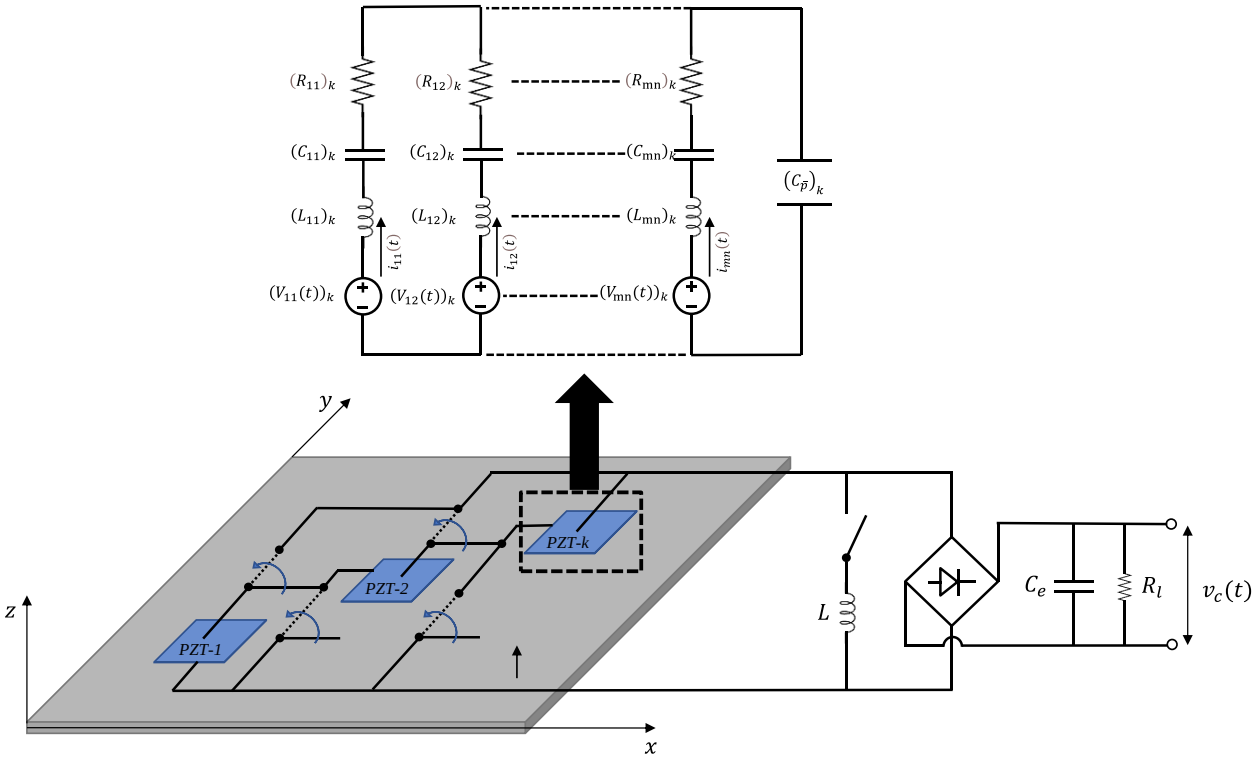

Figure 1. Multiple piezo-patch energy harvesters attached on a thin plate integrated with an SSHI circuit: The piezo-patches are connected in series and can also be connected in parallel by switching the terminals in the arrow direction. The zoomed-out dashed rectangle shows the equivalent circuit model (ECM) representation of k-th piezo-patch.

2.1. Electromechanical equations for series configuration

The representation for k piezo-patches which are represented as dependent current sources and connected in series with an SSHI circuit is shown in Figure 2. Each piezo-patch has an internal capacitance of $(C_p)_k$. The electrical circuit equation for each PEH can be shown as:

$$(C_p)_k \frac{\mathrm{d}\, v_k^s(t)}{dt} + i_c^s(t) = i_k^s(t) \tag{1}$$

where $k = 1,2,\ldots,n_p$, $v_k^s(t)$ is the voltage across kth piezo-patch, $i_c^s(t)$ is the current passing into the SSHI circuit. The internal capacitance of the kth piezo-patch can be expressed as:

$$(C_p)_k = (\bar{\varepsilon}_{33}^S)_k \frac{(l_p)_k (w_p)_k}{(h_p)_k} \tag{2}$$

where $(\bar{\varepsilon}_{33}^S)_k$ is the permittivity at constant strain, $(l_p)_k$ is the length, $(w_p)_k$ is the width, $(h_p)_k$ is the thickness of the kth piezo-patch.

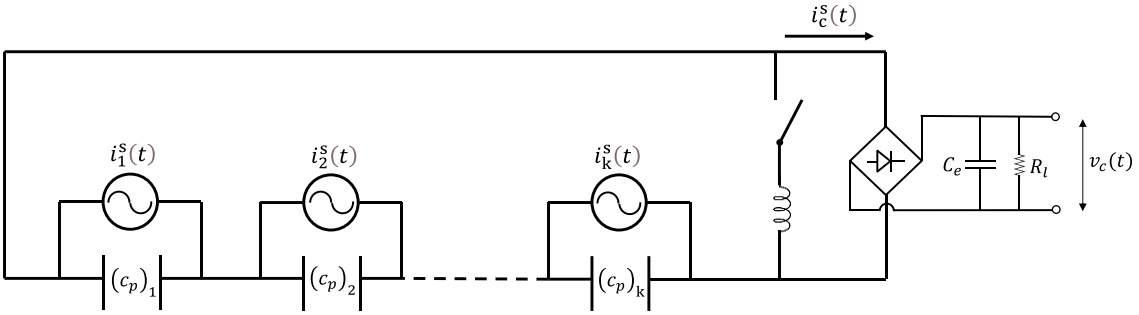

Figure 2. Electrical schematic of series connection of MPEHs integrated with an SSHI circuit.

From (Aridogan et al., 2014b), the electromechanically coupled equations in modal coordinates for series configuration are:

$$\frac{d^2\eta_{mn}^s(t)}{dt^2} + 2\zeta_{mn}\omega_{mn}\frac{d\eta_{mn}^s(t)}{dt} + \omega_{mn}^2\eta_{mn}^s(t) - \sum_{k=1}^{n_p}(\tilde{\theta}_{mn})_k v_k^s(t) = f_{mn}(t) \tag{3}$$

$$\sum_{\mathrm{n=1}}^{\infty}\sum_{\mathrm{m=1}}^{\infty}(\tilde{\theta}_{mn})_k \frac{d\eta_{mn}^s(t)}{dt} + (C_p)_k \frac{dv_k^s(t)}{dt} + i_c^s(t) = 0 \tag{4}$$

where the mechanical part is represented Eqn. (3), and the electrical part is represented in Eqn. (4). ζ_{mn} and ω_{mn} represents the modal damping ratio and the undamped natural frequency, respectively for the *mn*-th mode. The transverse force in modal coordinates, $f_{mn}(t)$ is (Aridogan et al., 2014b):

$$f_{mn}(t) = f(t)\phi_{mn}(x_0, y_0) \tag{5}$$

Using equations (1) and (4), the current source of the kth piezo patch for series configuration can be found as:

$$i_k^s(t) = -\sum_{n=1}^{\infty}\sum_{m=1}^{\infty}(\tilde{\theta}_{mn})_k \frac{d\eta_{mn}^s(t)}{dt} \tag{6}$$

where $\eta_{mn}^s(t)$ is the modal coordinate of the plate for the *mn*-th mode and the electromechanical coupling term $(\tilde{\theta}_{mn})_k$ is:

$$(\tilde{\theta}_{mn})_k = \theta_k \int_{y_{k,1}}^{y_{k,2}} \int_{x_{k,1}}^{x_{k,2}} \left[\frac{\partial^2 \phi_{mn}(x,y)}{\partial x^2} + \frac{\partial^2 \phi_{mn}(x,y)}{\partial y^2}\right] dxdy \tag{7}$$

where $\phi_{mn}(x, y)$ is the mass-normalized eigenfunction of the *mn*-th vibration mode at (x, y) coordinate, electromechanical term for the kth piezo-patch is $\theta_k = (h_{\mathrm{pc}})_k(\bar{e}_{31})_k$. Here, $(\bar{e}_{31})_k$ represents the effective piezoelectric constant and $(h_{\mathrm{pc}})_k$ represents the distance of the center layer of the kth piezo-patch from the reference surface at the location of the kth piezo-patch. Also, $x_{k,1}$ and $x_{k,2}$, represents the x coordinates and $y_{k,1}$and $y_{k,2}$ represents the y coordinates of the kth piezo-patch.

2.2. Electromechanical equations for parallel configuration

The representation for k piezo-patches, which are represented as dependent current sources and connected in parallel with an SSHI circuit is shown in Figure 3.

$$\frac{\mathrm{d}\, v^p(t)}{dt}\sum_{k=1}^{n_{\bar{p}}}(C_{\bar{p}})_k + i_c^p(t) = \sum_{k=1}^{n_{\bar{p}}} i_k^p(t) \tag{8}$$

In Equation (8), $v^p(t)$, $i_c^p(t)$ represents the voltage across each piezo-patch electrodes and the current passing through the SSHI circuit, respectively. The equivalent piezoelectric capacitance, which is denoted as $(C_{\bar{p}})_k$ is same as (2). The current source equation can be written as:

$$i_k^p(t) = -\sum_{n=1}^{\infty}\sum_{m=1}^{\infty}(\tilde{\theta}_{mn})_k \frac{d\eta_{mn}^p(t)}{dt} \tag{9}$$

where, $\eta_{mn}^{p}(t)$ is the modal coordinate for the *mn*-th mode and the electromechanical coupling term $(\tilde{\theta}_{mn})_k$ is same as (7).

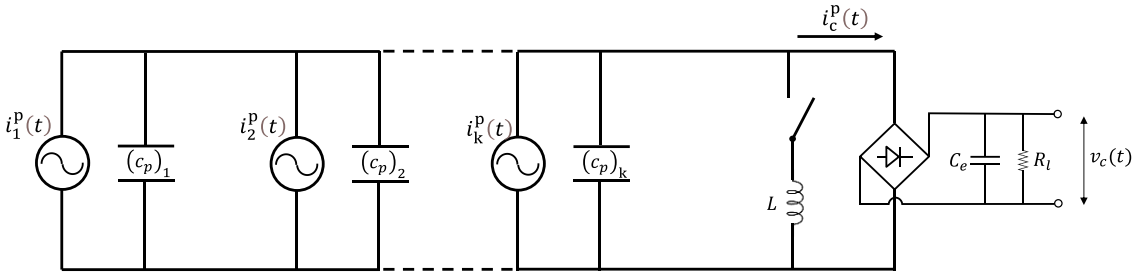

Figure 3. Electrical schematic of parallel connection of MPEHs integrated with an SSHI circuit.

From (Aridogan et al., 2014b), the electromechanically coupled equations in modal coordinates for parallel configuration can be expressed as

$$\frac{d^2\eta_{mn}^{p}(t)}{dt^2} + 2\zeta_{mn}\omega_{mn}\frac{d\eta_{mn}^{p}(t)}{dt} + \omega_{mn}^2\eta_{mn}^{p}(t) - \sum_{k=1}^{n_p}(\tilde{\theta}_{mn})_k v_k^s(t) = f_{mn}(t) \tag{10}$$

$$\sum_{k=1}^{n_{\bar{p}}}\sum_{n=1}^{\infty}\sum_{m=1}^{\infty}(\tilde{\theta}_{mn})_k\frac{d\eta_{mn}^{p}(t)}{dt} + \frac{dv^p(t)}{dt}\sum_{k=1}^{n_{\bar{p}}}(C_{\bar{p}})_k + i_c^p(t) = 0 \tag{11}$$

The transverse force in modal coordinates which is represented as $f_{mn}(t)$ is same as (5).

The equivalent circuit model (ECM) of the plate coupled with the *k*-th piezo-patch is also shown in Figure 1. In ECM, each branch represents a vibration mode, where there are $m \times n$ modes in total. Each set of secondary-order circuits can also be represented by dependent current sources in the literature (Aghakhani and Basdogan, 2017) where each current source contains a voltage source, an inductor, a capacitor, and a resistor to represent each mode. As every schematic represents a single PEH, this schematic needs to be repeated for the MPEH case.

After applying Kirchhoff's voltage law and analogy with the electromechanically coupled equations in modal coordinates for series and parallel configurations (Aridogan et al., 2014b), the second-order equivalent circuit model parameters and the mechanical counterparts can be found as shown in Table 1 (Aghakhani and Basdogan, 2017) for MPEHs.

Table 1. Equivalent circuit parameters and their analogy with the mechanical domain for MPEHs.

Equivalent circuit parameters for the *mn*-th vibration mode of *k*-th piezo-patch harvester	Mechanical counterparts

Voltage source: $(v_{mn}(t))_k$	$-\frac{f_{mn}(t)}{\sum_{k=1}^{n_p}(\tilde{\theta}_{mn})_k}$
Electrical current: $(i_{mn}(t))_k$	$-(\tilde{\theta}_{mn})_k \dot{\eta}_{mn}^{p}(t)$ (parallel) $-(\tilde{\theta}_{mn})_k \dot{\eta}_{mn}^{s}(t)$ (series)
Inductance: $(L_{mn})_k$	$\frac{1}{(\tilde{\theta}_{mn})_k \sum_{k=1}^{n_p}(\tilde{\theta}_{mn})_k}$
Resistance: $(R_{mn})_k$	$\frac{2\zeta_{mn}\omega_{mn}}{(\tilde{\theta}_{mn})_k \sum_{k=1}^{n_p}(\tilde{\theta}_{mn})_k}$
Capacitance: $(C_{mn})_k$	$\frac{(\tilde{\theta}_{mn})_k \sum_{k=1}^{n_p}(\tilde{\theta}_{mn})_k}{{\omega_{mn}}^2}$

3. Networked Configurations

In this section, four different networks for three piezoelectric energy harvesters are presented. These configurations are explained in the proceeding sections. The schematic of the SSHI circuit used in the simulations is presented in Figure 4, which is a type of parallel-SSHI (p-SSHI). Diodes used in this circuit are characterized as they have a forward voltage drop as 0.25 V, to represent the BAT46W fast recovery Schottky diodes. The SSHI circuit is connected to a piezoelectric patch, which is shown as a current source in Figure 4.

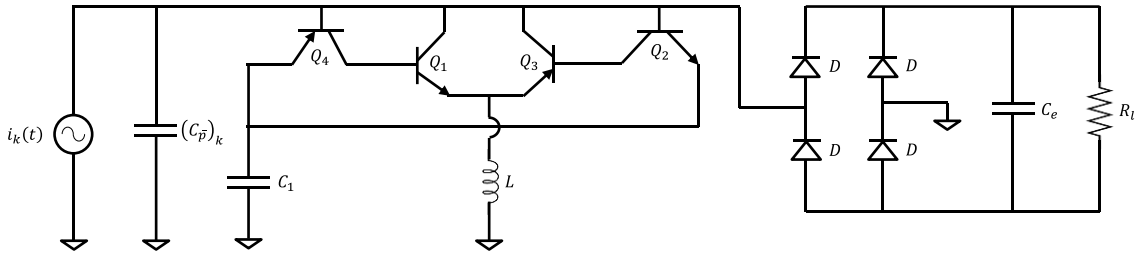

Figure 4. Schematic of the SSHI circuit connected to a piezoelectric patch.

The network configurations considered in this study is presented in Figure 5.

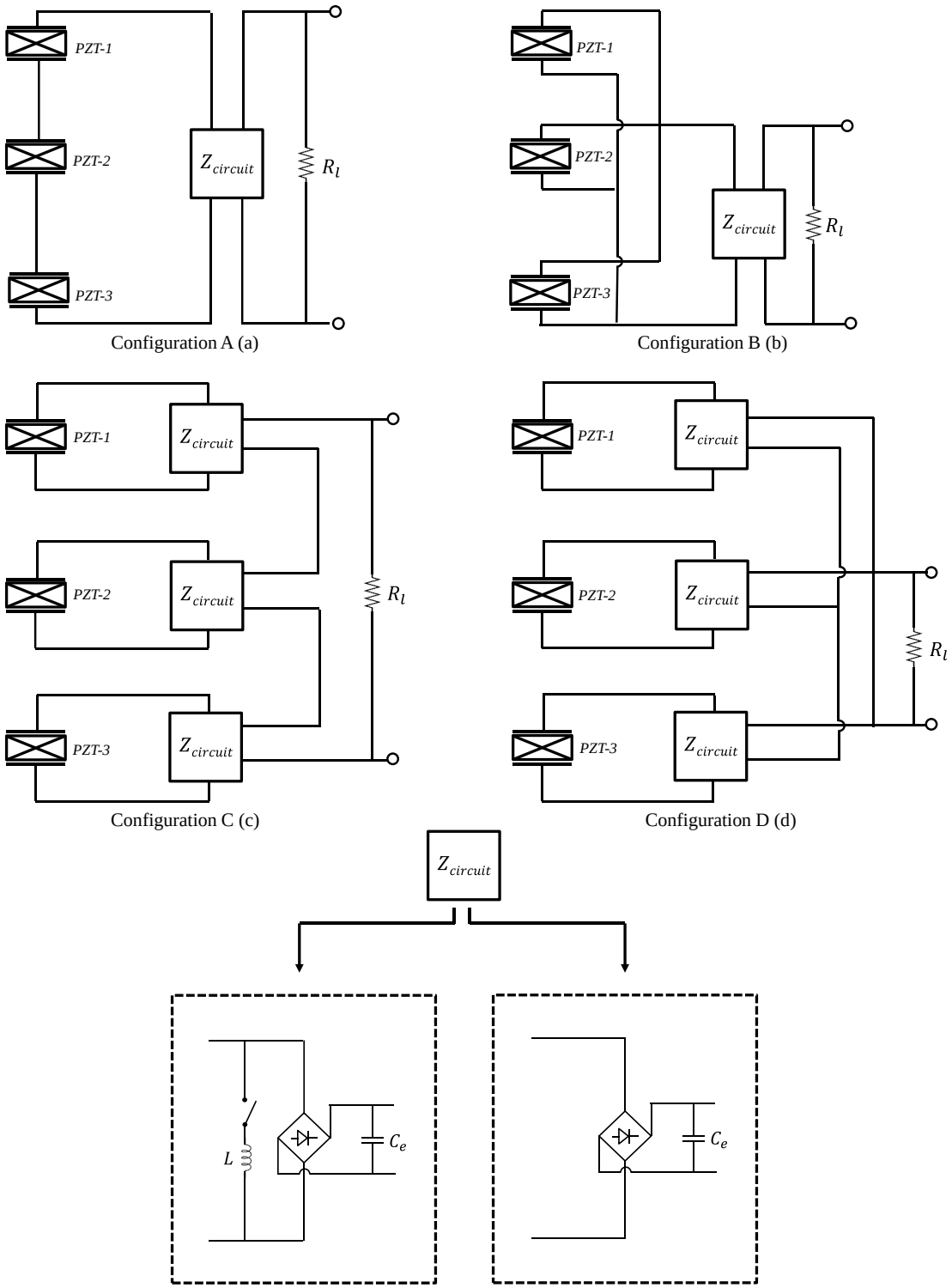

Figure 5. The circuit models for all configurations and the expansion of $Z_{circuit}$. (a) Configuration A: Multiple series patches – single rectifier/SSHI. (b) configuration B: Multiple parallel patches – single SSHI. (c) Configuration C: Multiple patches – multiple series rectifiers/SSHIs. (d) Configuration D: Multiple patches – multiple parallel rectifiers/SSHIs. (e) SSHI and rectifier circuit components.

In configuration A, presented in Figure 5 (a), three piezo-patches are connected in series and a single rectifier/SSHI circuit is integrated into the series configuration of the piezo-patches. This configuration will be a reference for comparison with configurations where multiple rectifiers/SSHIs are used in the upcoming sections.

Figure 5 (b) presents configuration B, where three piezo-patches are connected in parallel, and a single rectifier/SSHI circuit is integrated into the parallel configuration of the piezo-patches. As there is only a single rectifier/SSHI circuit, all three piezo-patches are contributing to a single waveform in this configuration, just like configuration A.

In Figure 5 (c), configuration C is presented where each piezo-patch has been integrated with a rectifier/SSHI circuit, and the output of those rectifier/SSHI circuits are connected in series. There are separate capacitors for each piezo-patch and the output voltage is the sum of the outputs of three SSHI circuits. Due to this summation, this configuration is expected to result in higher voltage outputs for higher load resistances.

Configuration D, which consists of multiple rectifier/SSHI circuits connected in parallel is presented in Figure 5 (d). Similar to configuration C, there are separate capacitors for each piezo-patch, and the output voltage on R_l is expected to be determined by the most dominant piezo-patch for that particular frequency.

4. Experimental Setup and Model Verifications

The experimental setup to verify the energy harvesting performance of the configurations is presented in Figure 6. A rectangular aluminum plate is used as the host plate, and all four edges are clamped by tightening the screws on the clamping frame. Three transversely isotropic piezoceramic patches (T105-A4E-602 manufactured by Piezo Systems, Inc.) are bonded as piezo-patch energy harvesters on the host plate. Since the locations of the piezo-patches need to observe all the modes in the frequency of interest to reflect the effect of different configurations on the performance, they are specifically located at the strain regions of the plate (one piezo-patch, at least, covers the maximum strain region of one of the resonance modes). All the vibration modes in the frequency range of interest are considered by using multiple piezo-patches. The aluminum plate is excited by a modal shaker at 0.085 m to the left and 0.085 m to the up from the right bottom corner, and the dynamic point force acting on the plate is measured by a force transducer (PCB 208C02). The transverse velocity outputs are measured by a laser Doppler vibrometer (Polytec PDV 100). At the first stage of the experiment, AC input - AC output analyses were performed by applying a linear sine sweep for 40-195 Hz range for open-circuit ($R_l = 1M\Omega$) condition. For the second stage, the configuration performances have been analyzed by applying sine sweep at the narrow bandwidths for each mode one-by-one, where the bandwidths are selected as the power outputs are above a considerable level. The sweep rate has been chosen to be slow enough to allow the smoothing capacitor charge and fast enough to prevent unnecessarily big experimental data to be saved.

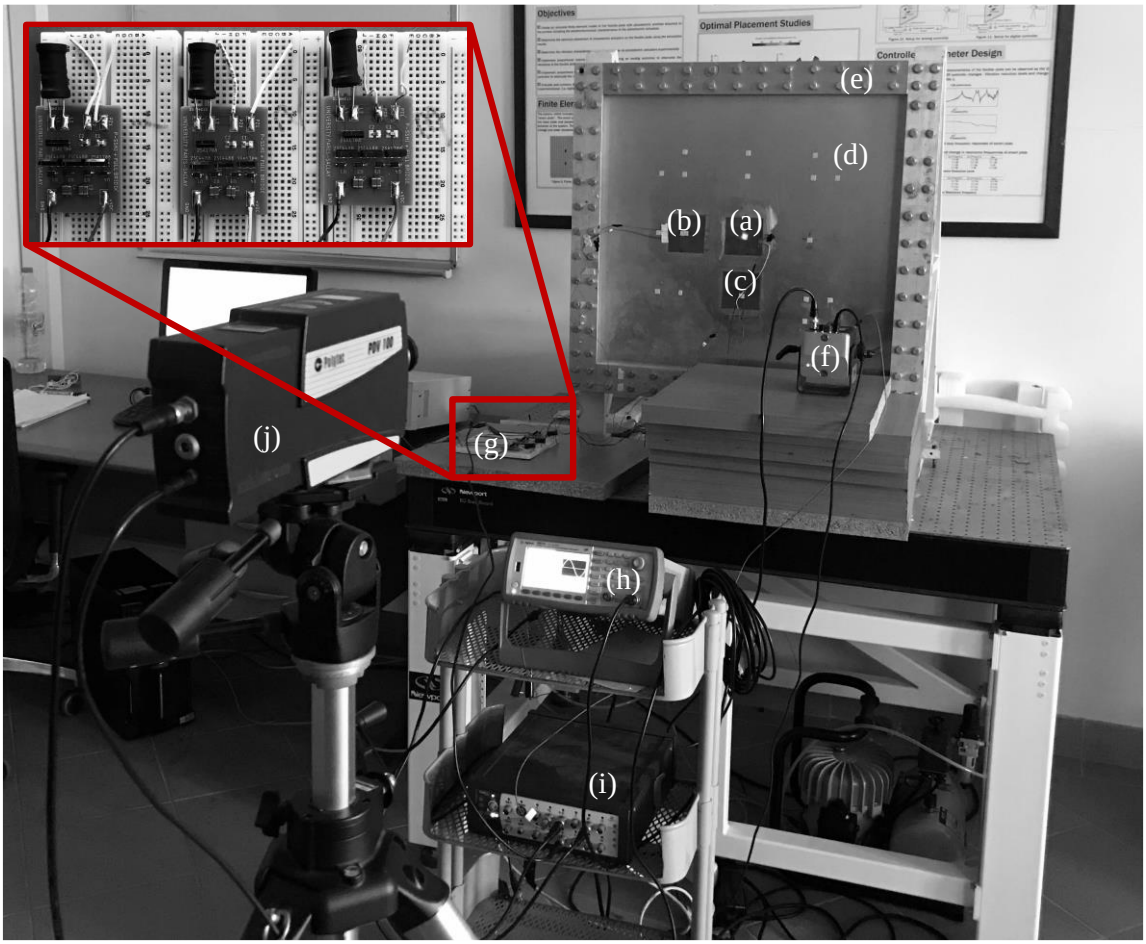

Figure 6. Experimental setup: (a) PZT-1, (b) PZT-2, (c) PZT-3, (d) aluminum host plate, (e) clamping frames, (f) shaker with a force transducer, (g) SSHI circuits, (h) signal generator, (i) data acquisition unit and (j) laser vibrometer.

The geometric and material properties of the host plate and the piezoceramics are presented in Table 2.

Table 2. Geometric and material properties of the host plate and the piezoceramics.

Properties	Aluminum Plate	Piezoceramic
Length (mm)	580	72.4
Width (mm)	540	72.4
Thickness (mm)	1.9	0.267
Young's Modulus (GPa)	65.1	66
Mass Density (kg m^{-3})	2575	7800
Piezoelectric Constant d^{31} (pm V^{-1})	-	-190
Permittivity Constant $\bar{\varepsilon}_{33}^{S}$ (Nf m^{-1})	-	10.38

4.1. AC input – AC output verifications

The AC input – AC output results have been compared and presented in Figure 7 for open-circuit ($R_l = 1M\Omega$) condition both for experimental and numerical analyses from 40 Hz to 195 Hz. The modal damping ratios are extracted from the experimental voltage FRFs using half-power point (HPP) method and an equivalent circuit model is developed considering the first 20 modes of the plate to be used in the numerical analyses which are performed in the electrical circuit simulation software LTspice. As it can be observed, the LTspice simulations match the experimental analyses in terms of the natural frequencies and the voltage outputs firmly, except the trivial frequency shift in the third mode. The discrepancies between the numerical and experimental models can be explained by the difficulty of achieving a perfect clamping and the experimental room conditions, which affect the modal parameters. Also, the aluminum plate parameters are taken from material tables, and these can be slightly different than the plate used in the experiments. The modal damping ratios of the model for the first five modes are 0.004, 0.004, 0.002, 0.001 and 0.005, respectively.

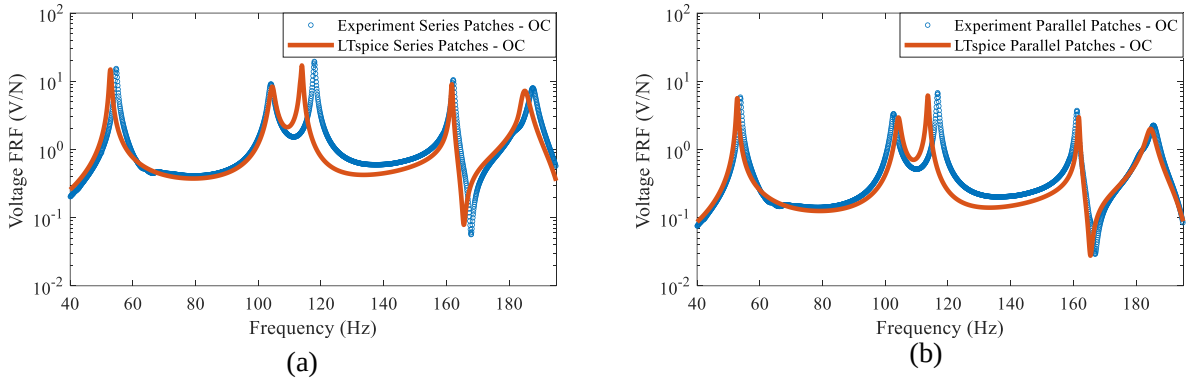

Figure 7. Comparison of experimental and numerical model for the AC input- AC output case. Three piezo-patches are connected in series (a) and parallel (b) configurations, and a load resistance of 1MΩ is connected to the output of the configurations.

4.2. AC input – DC output verifications

In this section, the simulation and experimental results for three piezo-patches attached to a thin plate and integrated with the aforementioned networked rectifier/SSHI configurations are shared where the generated ECM and the SSHI configurations are integrated into LTspice. For the AC input – DC output numerical analyses, the standard rectifier circuit and the SSHI circuit in Figure 5 (e) are used for all configurations. Voltage frequency response functions (FRFs) are presented in Figure 8 for the four different networked SSHI configurations, where the thirteen different resistive loads ranging from 1 kΩ to 1 MΩ are used for the analyses. The plate is excited with a harmonic force, and the output voltages are measured. The LTspice model of the SSHI circuit has been integrated with the ECM of the plate, where the circuit elements are chosen similar to the experimental SSHI circuit. Despite some assumptions made in the diode and SSHI circuit modeling, the results obtained from LTspice simulations closely match the experimental results. It can be observed that the natural frequency of the plate structure has been shifted by an amount

in configuration C and D. This is due to the experimental room conditions where the changes in the temperature of the room change the natural frequency of the structure (Cai et al., 2021). Also, there are several studies about the effect of temperature on the piezoelectric energy harvesting, which explains the small discrepancies between numerical analyses and the experimental analyses (Kim et al., 2011, Yang et al., 2017).

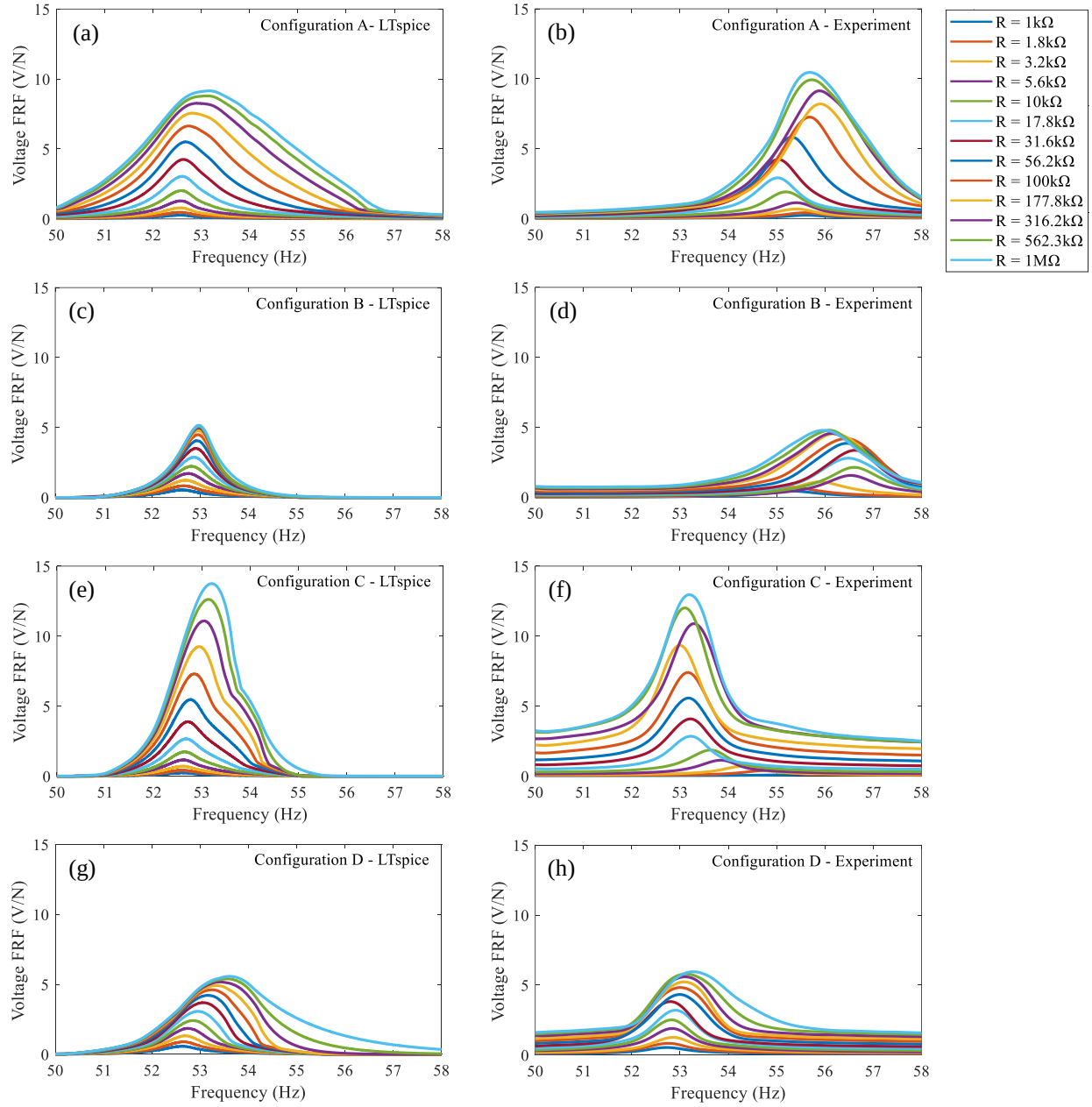

Figure 8. LTspice and experiment results presenting the variations of voltage FRFs (V/N) of the four different configurations for networked SSHI; configuration A: LTspice (a) and experiment (b); configuration B: LTspice (c) and experiment (d); configuration C: LTspice (e) and experiment (f) and configuration D: LTspice (g) and experiment (h) for thirteen load resistances ranging from 1kΩ to 1MΩ.

Considering the AC input – AC output results in Figure 7 and AC input – DC output results in Figure 8, it can be said that the numerical model captures the modes and the trend of voltage outputs for the first five modes and therefore can be used as a useful tool to evaluate the power output for the possible future case studies as well.

To assess the performance of the networked SSHI configurations, one can use the performance of the networked rectifier configurations as a reference. Since the utilization of multiple rectifiers/SSHI circuits and different load resistances induce a slight variation in resonance frequency, instead of directly calculating the power value at a specific frequency, frequency sweeps have been performed for narrowed frequency ranges for each mode, and the peak power values are captured. These peak powers of the four different networked rectifier and networked SSHI configurations versus varying thirteen resistances from 1kΩ to 1MΩ have been presented in Figure 9.

All three piezo-patches have the same internal capacitance, which is 247 nF. As stated by Erturk and Inman (2011), the equivalent piezoelectric capacitance and the optimum load resistance have an inverse proportion. This is the reason why configuration A and C responds with higher peak powers in higher load resistances compared to configuration B and D, which respond better in lower load resistances in most of the cases. This phenomenon can be useful to match the impedance of the sensor device to be powered.

The improvement of the peak power outputs after using networked SSHI instead of networked rectifier is tabulated in Table 3. The results indicate that the networked SSHI configurations outperform networked rectifier configurations when the average power improvements are accounted for in experiments for each configuration. In order to compare the performances of the different networked SSHI configurations, the experimental peak power outputs of each configuration for the first five modes are presented in Table 4. The optimal configuration is determined by comparing the peak power levels of each configuration and expressing their power improvement percentage with configuration A as the reference. As it can be observed, the peak power values are far smaller for single SSHI configurations compared to multiple SSHI configurations in some of the modes. The reason for this is the charge cancelation since the collected charge output on the electrode layers of the piezo-patches is determined by the strain distribution, and with the current positions of the piezo-patches, the charges might cancel each other for these modes (Aridogan et al., 2014b). In the cases where multiple piezo-patches are connected, one should consider the voltage phases if a single SSHI is to be used. The imaginary part of the voltage FRF of each patch should match in terms of their signs to maximize the voltage output, thus power output. For the modes where there is negligible charge cancelation, e.g., first mode, the benefit of multiple SSHI circuits disappears. In addition, due to the voltage drop from the non-linear diodes in the SSHI circuits, the harvesting performance is affected negatively in terms of power outputs, as the voltage drop will be approximately three times higher than the single SSHI circuit cases. As charge cancelation occurs especially in the higher

modes due to the opposite signs of strain distribution under the piezoelectric patches, configuration C and D result in higher power outputs.

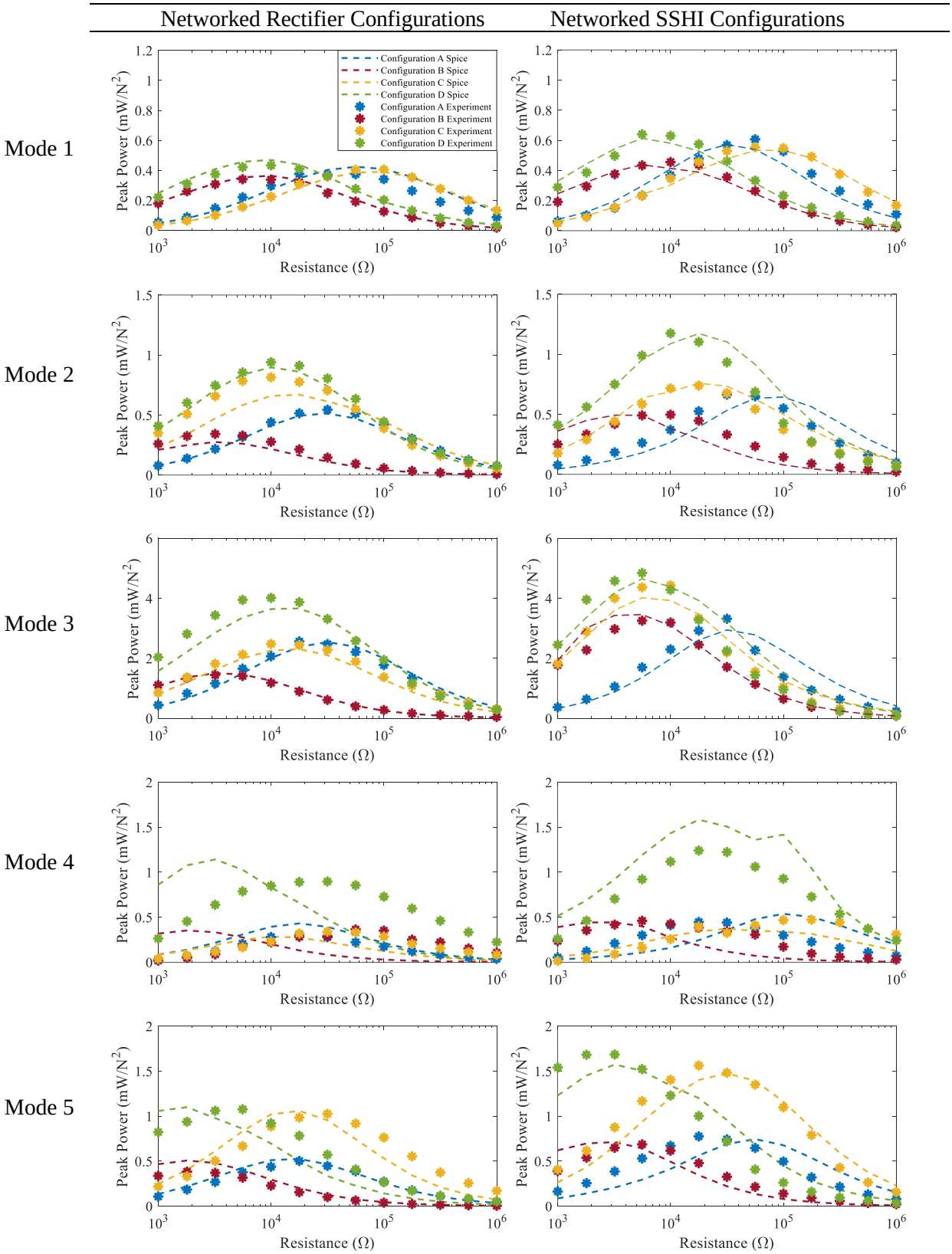

Figure 9. Comparison of peak power outputs of the four configurations of networked rectifier and networked SSHI versus varying resistances from 1 kΩ to 1 MΩ for the first five modes; both experimental and numerical results.

Table 3. Improvement/deterioration of the experimental peak power outputs after using networked SSHI circuit instead of networked rectifier circuit.

Modes and Average Improvement	Configuration A Peak Power Improvement (%)	Configuration B Peak Power Improvement (%)	Configuration C Peak Power Improvement (%)	Configuration D Peak Power Improvement (%)
Mode 1 (53.9 Hz)	61	34	37	48
Mode 2 (104.9 Hz)	22	46	-9	25
Mode 3 (114.7 Hz)	29	126	78	21
Mode 4 (161.5 Hz)	46	26	37	38
Mode 5 (185.7 Hz)	55	79	52	56
Average Improvement	42.6	62.2	39.0	37.6

Table 4. Experimental peak power outputs of the four networked SSHI configurations.

Modes	Configuration A Peak Power (mW/N^2)	Configuration B Peak Power (mW/N^2)	Configuration C Peak Power (mW/N^2)	Configuration D Peak Power (mW/N^2)	The Best Configuration and Improvement (%) (Configuration A as reference)
Mode 1 (53.9 Hz)	0.61	0.45	0.55	0.64	D (4.9)
Mode 2 (104.9 Hz)	0.66	0.50	0.74	1.18	D (78.8)
Mode 3 (114.7 Hz)	3.32	3.25	4.43	4.84	D (45.8)
Mode 4 (161.5 Hz)	0.44	0.46	0.47	1.24	D (181.8)
Mode 5 (185.7 Hz)	0.78	0.68	1.56	1.68	D (115.4)

5. Conclusion

In this study, four different networked rectifier and networked SSHI configurations were presented. The motivation of this study is to assess the performance of the networked SSHI configurations compared to networked rectifier configurations. For this purpose, four different networked rectifier/SSHI configurations are presented, where two of these configurations include a single rectifier/SSHI circuit, and the other two configurations include separate rectifier/SSHI circuits for each patch. The three piezo-patches are bonded with the aluminum host plate and equivalent circuit model of the electromechanical system is developed analytically and embedded in LTspice software such that the electromechanical system can be integrated with non-linear circuits. Four configurations are considered where single and multiple rectifier/SSHI circuits are integrated with the multiple piezo-patches. Later, the performances of each configuration are evaluated under harmonic excitation in terms of peak power outputs, and the optimal load resistances are identified. The experimental results are compared in relation to the peak power changes observed when SSHI circuits are employed instead of rectifier circuits in networked configurations. The results show that the SSHI circuits significantly enhance the output power when compared to the rectifier circuits in the networked configurations, especially in configuration B, by 62.2%. Subsequently, the results are compared in terms of the peak power outputs of the four different networked SSHI configurations. According to the results, the power output has increased by 4.9%, 78.8%, 45.8%, 181.8%, and 115.4% for the first, second, third,

fourth, and fifth modes, respectively, when configuration D is used rather than configuration A. The results show that using multiple SSHI circuits significantly boosts the power output for the modes of charge cancelation. Also, for these modes, one can choose between configuration C and configuration D depending on the impedance of the sensor device by accounting for the power output difference between the two configurations. In most of the modes, the series configurations outperformed the parallel ones for the higher load resistances. This is due to the reverse relationship between the equivalent capacitance value and the load resistance. Therefore, one may choose the optimal configuration depending on the impedance of the device to be powered. For higher equivalent impedances, choosing Configuration C makes sense while for lower load resistances, Configuration D is a better choice. Lastly, when multiple piezopatches are used, charge cancellation is inevitable, therefore using respective SSHI circuits is beneficial, and regardless of the configuration type, networked SSHI circuits outperformed networked rectifier circuits overall.

Acknowledgment

The authors thank Professor E. Lefeuvre for supplying the SSHI circuits and his valuable inputs.

Declaration of conflicting interests

The author(s) declared no potential conflicts of interest with respect to the research, authorship, and/or publication of this article.

Funding

The author(s) received no financial support for the research, authorship, and/or publication of this article.

ORCID iDs

Engin Tarhan https://orcid.org/0000-0002-6756-4850

Seyed Morteza Hoseyni https://orcid.org/0000-0002-9057-1223

Amirreza Aghakhani https://orcid.org/0000-0002-4301-4053

Ipek Basdogan https://orcid.org/0000-0001-9092-5856

References

Aghakhani, A. & Basdogan, I. 2017. Equivalent impedance electroelastic modeling of multiple piezo-patch energy harvesters on a thin plate with AC–DC conversion. *IEEE/ASME Transactions on Mechatronics,* 22**,** 1575-1584.

Anton, S. R. & Sodano, H. A. 2007. A review of power harvesting using piezoelectric materials (2003–2006). *Smart materials and Structures,* 16**,** R1.

Aridogan, U., Basdogan, I. & Erturk, A. 2014a. Analytical modeling and experimental validation of a structurally integrated piezoelectric energy harvester on a thin plate. *Smart Materials and Structures,* 23**,** 045039.

Aridogan, U., Basdogan, I. & Erturk, A. 2014b. Multiple patch–based broadband piezoelectric energy harvesting on plate-based structures. *Journal of Intelligent Material Systems and Structures,* 25**,** 1664-1680.

Aridogan, U., Basdogan, I. & Erturk, A. 2016. Random vibration energy harvesting on thin plates using multiple piezopatches. *Journal of Intelligent Material Systems and Structures,* 27**,** 2744-2756.

Bayik, B., Aghakhani, A., Basdogan, I. & Erturk, A. 2016. Equivalent circuit modeling of a piezo-patch energy harvester on a thin plate with AC–DC conversion. *Smart Materials and Structures,* 25**,** 055015.

Cai, Y., Zhang, K., Ye, Z., Liu, C., Lu, K. & Wang, L. 2021. Influence of temperature on the natural vibration characteristics of simply supported reinforced concrete beam. *Sensors,* 21**,** 4242.

Chao, P. C.-P. 2011. Energy harvesting electronics for vibratory devices in self-powered sensors. *IEEE Sensors Journal,* 11**,** 3106-3121.

Elvin, N. G. & Elvin, A. A. 2009a. A coupled finite element—circuit simulation model for analyzing piezoelectric energy generators. *Journal of intelligent material systems and structures,* 20**,** 587-595.

Elvin, N. G. & Elvin, A. A. 2009b. A general equivalent circuit model for piezoelectric generators. *Journal of Intelligent Material Systems and Structures,* 20**,** 3-9.

Erturk, A. & Inman, D. J. 2008. A distributed parameter electromechanical model for cantilevered piezoelectric energy harvesters. *Journal of vibration and acoustics,* 130.

Erturk, A. & Inman, D. J. 2009. An experimentally validated bimorph cantilever model for piezoelectric energy harvesting from base excitations. *Smart materials and structures,* 18**,** 025009.

Erturk, A. & Inman, D. J. 2011. *Piezoelectric energy harvesting*, John Wiley & Sons.

Erturk, A., Tarazaga, P. A., Farmer, J. R. & Inman, D. J. 2009. Effect of strain nodes and electrode configuration on piezoelectric energy harvesting from cantilevered beams.

Friswell, M. I., Ali, S. F., Bilgen, O., Adhikari, S., Lees, A. W. & Litak, G. 2012. Non-linear piezoelectric vibration energy harvesting from a vertical cantilever beam with tip mass. *Journal of Intelligent Material Systems and Structures,* 23**,** 1505-1521.

Graf, C., Maas, J. & Schapeler, D. Energy harvesting cycles based on electro active polymers. Electroactive Polymer Actuators and Devices (EAPAD) 2010, 2010. SPIE, 362-373.

Guyomar, D., Badel, A., Lefeuvre, E. & Richard, C. 2005. Toward energy harvesting using active materials and conversion improvement by nonlinear processing. *IEEE transactions on ultrasonics, ferroelectrics, and frequency control,* 52**,** 584-595.

Hoseyni, S. M., Şİmşek, M., Aghakhani, A., Lefeuvre, E. & Basdogan, I. 2023. Multimodal piezoelectric energy harvesting on a thin plate integrated with SSHI circuit: an analytical and experimental study. *Smart Materials and Structures*.

Howells, C. A. 2009. Piezoelectric energy harvesting. *Energy Conversion and Management,* 50**,** 1847-1850.

Jiang, S., Li, X., Guo, S., Hu, Y., Yang, J. & Jiang, Q. 2005. Performance of a piezoelectric bimorph for scavenging vibration energy. *Smart materials and structures,* 14**,** 769.

Johnson, T. J., Charnegie, D., Clark, W. W., Buric, M. & Kusic, G. Energy harvesting from mechanical vibrations using piezoelectric cantilever beams. Smart Structures and Materials 2006: Damping and Isolation, 2006. SPIE, 81-92.

Junior, C. D. M., Erturk, A. & Inman, D. J. 2009. An electromechanical finite element model for piezoelectric energy harvester plates. *Journal of Sound and Vibration,* 327**,** 9-25.

Kim, S.-B., Park, J.-H., Ahn, H., Liu, D. & Kim, D.-J. 2011. Temperature effects on output power of piezoelectric vibration energy harvesters. *Microelectronics journal,* 42**,** 988-991.

Lee, C., Lim, Y. M., Yang, B., Kotlanka, R. K., Heng, C.-H., He, J. H., Tang, M., Xie, J. & Feng, H. 2009. Theoretical comparison of the energy harvesting capability among various electrostatic mechanisms from structure aspect. *Sensors and Actuators A: Physical,* 156**,** 208-216.

Lee, S., Youn, B. D. & Giraud, M. Designing energy harvesting skin structure utilizing outdoor unit vibration. International Design Engineering Technical Conferences and Computers and Information in Engineering Conference, 2010. 713-723.

Lefeuvre, E., Badel, A., Richard, C. & Guyomar, D. High-performance piezoelectric vibration energy reclamation. Smart Structures and Materials 2004: Smart Structures and Integrated Systems, 2004. SPIE, 379-387.

Lefeuvre, E., Badel, A., Richard, C. & Guyomar, D. 2005. Piezoelectric energy harvesting device optimization by synchronous electric charge extraction. *Journal of intelligent material systems and structures,* 16**,** 865-876.

Li, H., Liu, D., Wang, J., Shang, X. & Hajj, M. R. 2020. Broadband bimorph piezoelectric energy harvesting by exploiting bending-torsion of L-shaped structure. *Energy Conversion and Management,* 206**,** 112503.

Li, Y., Guyomar, D. & Richard, C. Influence of the topology for a networked SSHI piezoelectric harvesting configuration. Active and Passive Smart Structures and Integrated Systems 2013, 2013. SPIE, 43-57.

Long, Z., Li, P., Wang, X., Wang, B., Chung, H. S.-H. & Yang, Z. 2021. A self-powered P-SSHI array interface for piezoelectric energy harvesters with arbitrary phase difference. *IEEE Transactions on Industrial Electronics,* 69**,** 9155-9164.

Narita, F. & Fox, M. 2018. A review on piezoelectric, magnetostrictive, and magnetoelectric materials and device technologies for energy harvesting applications. *Advanced Engineering Materials,* 20**,** 1700743.

Ottman, G. K., Hofmann, H. F., Bhatt, A. C. & Lesieutre, G. A. 2002. Adaptive piezoelectric energy harvesting circuit for wireless remote power supply. *IEEE Transactions on power electronics,* 17**,** 669-676.

Pradeesh, E., Udhayakumar, S., Vasundhara, M. & Kalavathi, G. 2022. A review on piezoelectric energy harvesting. *Microsystem Technologies,* 28**,** 1797-1830.

Safaei, M., Sodano, H. A. & Anton, S. R. 2019. A review of energy harvesting using piezoelectric materials: state-of-the-art a decade later (2008–2018). *Smart Materials and Structures,* 28**,** 113001.

Shu, Y., Lien, I., Wu, W. & Shiu, S. Comparisons between parallel-and series-SSHI interfaces adopted by piezoelectric energy harvesting systems. Active and Passive Smart Structures and Integrated Systems 2009, 2009. SPIE, 117-128.

Sodano, H. A., Park, G. & Inman, D. 2004. Estimation of electric charge output for piezoelectric energy harvesting. *Strain,* 40**,** 49-58.

Torres, E. O. & Rincón-Mora, G. A. 2008. Electrostatic energy-harvesting and battery-charging CMOS system prototype. *IEEE Transactions on Circuits and Systems I: Regular Papers,* 56**,** 1938-1948.

Wang, L. & Yuan, F. 2008. Vibration energy harvesting by magnetostrictive material. *Smart Materials and Structures,* 17**,** 045009.

Wu, D., Guyomar, D. & Richard, C. A new global approach using a network of piezoelectric elements and energy redistribution for enhanced vibration damping of smart structure. Active and Passive Smart Structures and Integrated Systems 2013, 2013. SPIE, 251-265.

Yang, H., Guo, M., Wang, L., Hou, Y., Zhao, Q., Cao, D., Zhou, B. & Wang, D. 2017. Investigation on the factors influencing the performance of piezoelectric energy harvester. *Road materials and pavement design,* 18**,** 180-189.

Yang, Y. & Tang, L. 2009. Equivalent circuit modeling of piezoelectric energy harvesters. *Journal of intelligent material systems and structures,* 20**,** 2223-2235.

Zheng, X., Zhang, Z., Zhu, Y., Mei, J., Peng, S., Li, L. & Yu, Y. 2014. Analysis of energy harvesting performance for $ d_ {15} $ mode piezoelectric bimorph in series connection based on Timoshenko beam model. *IEEE/ASME Transactions on Mechatronics,* 20**,** 728-739.